PHYSICS AND CHEMISTRY OF SOLID STATE
V. 25, No. 4 (2024) pp. 871-879
Section: Physics

DOI: 10.15330/pcss.25.4.871-879

Vasyl Stefanyk Precarpathian National University

ФІЗИКА І ХІМІЯ ТВЕРДОГО ТІЛА
Т. 25, № 4 (2024) С. 871-879
Фізико-математичні науки

PACS: 62.20.de, 68.37.Ps, 68.60.Bs, 68.55.Ln, 78.30.j, 81.40.Jj

ISSN 1729-4428 (Print)
ISSN 2309-8589 (Online)

A.A. Korchoviy, P.M. Lytvyn, V.M. Dzhagan, O.Y. Gudymenko, K.V. Svezhentsova, M.S. Boltovets, V.V. Strelchuk, O.M. Kolesnikov, O.F. Isaieva, V.S. Yefanov, V.P. Melnik, B.M. Romanyuk

Nanomechanical and optical vibrations properties of vanadium oxide thin films obtained by multi-step deposition approach

V. Lashkaryov Institute of Semiconductors Physics, NAS of Ukraine, Kyiv, Ukraine, svezhentsova@ukr.net

Vanadium oxide thin films were fabricated using a multi-step deposition process involving magnetron sputtering and sequential annealing. The structural, vibrational, and nanomechanical properties of the films were investigated to elucidate the impact of phase composition on the performance of metal-insulator phase transition (MIT). X-ray diffraction (XRD) and Raman spectroscopy revealed a structural evolution from quasi-amorphous to nanocrystalline phases upon annealing, with transitions from VO_2 to textured V_4O_9 dominating the annealing process. The observed phase transition is accompanied by hardness increase from 0.9 GPa in the amorphous first layer to 11–18 GPa in all (crystalline) multi-layers. The hardening is attributed to development of well-ordered crystalline texture, which improved interatomic bonding and resistance to deformation. The vibrational Raman spectra obtained at various excitation wavelengths exhibit resonant sensitivity to different oxide phases, including the minority V_3O_7 phase not detectable by XRD and selective resonant probe of V_4O_9 phase only with 671 nm excitation. Temperature-dependent Raman and electrical resistivity measurements revealed superior MIT characteristics for samples with higher VO_2 content, despite the presence of other V_xO_y phases. These findings underscore the critical role of structural ordering in tuning the mechanical and functional properties of vanadium oxide films for advanced electronic and optical applications.

Keywords: Vanadium oxide, VO_2, V_4O_9, V_3O_7, Raman spectroscopy, X-ray diffraction, nanoindentation, metal-insulator transition, phase transition.

Received 25 July 2024; Accepted 06 December 2024.

Introduction

Vanadium oxides have been an area of intense research for a few decades, due to high promises of applications in uncooled microbolometers, thermochromic windows, catalysis, and many other [1-3]. The most attention has been paid to VO_2 phase, because it has an insulator-metal (MIT) transition at temperature of 68 C, with a suitable temperature coefficient of resistance (TCR) [4, 5]. The efforts of researchers and technologists have been mainly focused on obtaining the monophase and crystalline layers of VO_2 and reducing its transition temperature close to room temperature by inducing strain, changing V:O stoichiometry, or introducing dopants [2, 6 -10]. Although less intense, other oxides have been investigated, such as V_2O_3, V_3O_5, V_7O_{16}, V_4O_9, and V_2O_5 [11-14]. The importance of investigation of these oxides is twofold: to enable their identification as minor inclusions in the VO_2 layers and to find most efficient applications for these oxides. The V_2O_3 phase has very low resistivity, but the TCR value is too small to be applied as a microbolometer. The V_2O_5 phase has a large TCR value, but the resistivity is too large to be used for the microbolometer. Monoclinic VO_2 has low resistivity and high TCR value at the same time, however, due to the MIT phenomenon, hysteresis occurs in the temperature-resistance graph and stable operation is difficult in microbolometer. Therefore, mixed phase thin films of vanadium oxides, VO_2 and V_2O_5 [15], or to mix vanadium metal and V_2O_5 phase into a sandwich structure have been

studied [16]. Besides, obtaining vanadium oxide films as a mixture of two or more phases is much easier than phase-pure VO_2, but still can have competitive characteristics. For example, the mixed oxide VO_2:V_2O_5 (ratio of 36:64) exhibited TCR of 3.2 with a reasonable low resistance (120 Ohm/square) [15]. The films containing even more phases exhibited a TCR of 2-3 [17-20], which is comparable to pure VO_2 phase materials.

Another challenge is to obtain application-ready VO_2 (or other oxide) films of large enough thickness. Both the epitaxial and polycrystalline growth has certain critical thickness around 100-200 nm, beyond which the film loses its structural perfection or integrity with the substrate, while films up to 500 nm thick films are more suitable for applications. Various approaches have been demonstrated to attain thicker films of required quality: using various buffer layers (to reduce the strain in the film or improve adhesion), dopants, reducing the growth temperature [21, 22]. An original approach was proposed recently by or group – a multistep deposition of VO_2 films [9], which consists in several alternating cycles of deposition and annealing of layers of "subcritical" thickness (< 200 nm). In the present work, for the films obtained by multi-step deposition we investigate in detail the vibrational and nanomechanical properties.

Nanomechanical investigations of vanadium oxides (VO_x) have revealed critical insights into their mechanical and functional properties, especially in relation to structural phase transitions and synthesis conditions. The mechanical behavior of VO_2, for instance, is profoundly influenced by its metal-insulator transition (MIT), where the elastic modulus increases sharply by approximately 17 GPa as the material transitions from the insulating monoclinic phase to the metallic rutile phase. This highlights the potential for VO_2-based applications in electrical, mechanical, and sensor devices due to its unique coupled electronic and mechanical properties [23]. In situ investigations using advanced techniques, such as TEM-based stress-strain analysis of VO_2 nanowires, further demonstrate that tensile loading can modulate phase transition temperatures, providing a mechanism to actuate nanostructures or detect local thermal changes induced by external stimuli [24].

Nanomechanical tuning of VO_2 has also been achieved through controlled pressure application via scanning probe methods. Conductive AFM (C-AFM) studies reveal that applied pressures of approximately 5 GPa can reversibly induce the MIT at room temperature, enabling nanoscale switching between insulating and conductive states. This technique provides valuable insights into the coupled structural and electronic transitions in VO_2 and aids in the design of nanoscale oxide-based devices [25].

The mechanical properties of amorphous VO_x films are highly dependent on deposition conditions, such as the Ar_2 ratio during sputtering, which governs film density and microstructure. Hardness values range from 0.3 GPa for oxygen-rich porous films to 2.1 GPa for densely packed films deposited with higher argon content. Annealing induces phase transitions, such as the transformation of V_2O_5 from amorphous to polycrystalline states, leading to a marked increase in hardness from 3.2 GPa to 6.4 GPa, underscoring the impact of structural evolution on mechanical properties [26].

Our recent studies combining AFM nanoindentation, X-ray diffraction, and Raman spectroscopy have revealed order-of-magnitude increases in hardness and elastic modulus for VO_2-rich films compared to insulating oxides. These advances elucidate structure-property relationships, with systematic correlations between post-annealing, phase composition, and nanoscale mechanical performance. Innovations such as ion implantation further enhance mechanical properties through defect engineering, paving the way for optimized processing and a deeper understanding of nanoscale functionality in VO_x materials [17].

Experimental

VO_2 thin films were grown as described in the previous work of our group [27]. Magnetron sputtering of the VO_2 target at the background pressure of $(1…2)\cdot10^{-5}$ Torr and Ar (high purity 99.999%) pressure of $(2…4)\cdot10$ –3 Torr. The power of magnetron was kept at 50…70 W, and substrate temperature was 235 ± 15 °C. After deposition, the sample was annealed at 350 °C for 30 min in Ar ambient, and then next layer was deposited on top of the annealed layer. This procedure was repeated three times. After each deposition or annealing step, a part of sample was cut and numbered correspondingly (Table 1): 1,2,3 for samples after deposition and 1a, 2a, 3a for corresponding samples after annealing.

The crystal structure of the films was investigated using an X'Pert ProMPD X-ray diffractometer with the CuKα wavelength (λ = 0.15406 nm) in a sliding mode, with a scan step of 0.025 degrees. Attribution of XRD reflexed was performed according to the ICDD database (International Centre Diffraction Data). The film thickness was determined using a profilometer. The surface morphology and nano-mechanical properties of the films was studied using a scanning probe microscope NanoScope IIIa Dimension 3000TM. Surface relief measurements were performed in the tapping mode by using the ultrasharp silicon tips with the nominal radius of 8 nm. The nanoindentation mode and the cube corn diamond indenter with the apex radius 30 nm (135 N/m spring constant) were used for hardness and elasticity measurements.

The resistances and TCR values of the films were measured using a two-point probe system with a heating unit within the range 25 °C C to 90 °C.

Raman spectra were excited with λ_{exc} of 457, 532, 671, or 785 nm solid-state lasers, and acquired using a single-stage spectrometer MDR-23 (LOMO) equipped with a cooled CCD detector (Andor iDus 420, UK). The laser power density on the samples was less than 10^3 W/cm^2, to preclude any thermal or photo-induced modification of the samples. A spectral resolution for all excitation radiation wavelengths was about 4 cm^{-1}, as determined from the Si phonon peak width of a single-crystal Si substrate. The Si phonon peak position of 520.5 cm^{-1} was used as a reference for determining the position of the peaks in the Raman spectra acquired at different λ_{exc}'s. Variation of the sample temperature

during Raman measurements was performed using a home-built stage with temperature control from room temperature up to 190 °C.

I. Results and discussion

Structural and nanomechanical characterization

The X-ray diffraction patterns of sequentially deposited V_xO_y layers are presented in Fig. 1. After the deposition of the first layer (sample 1), the film exhibits a predominantly amorphous structure, as indicated by the broad halo in the low-angle region (curve 1). This amorphous nature is attributed to the initial layer's interaction with the silicon substrate, where the deposition conditions promote the formation of an amorphous film. At the interface, a thin nucleation layer containing small crystallites may exist, but their size and distribution are not sufficient to generate distinct diffraction peaks.

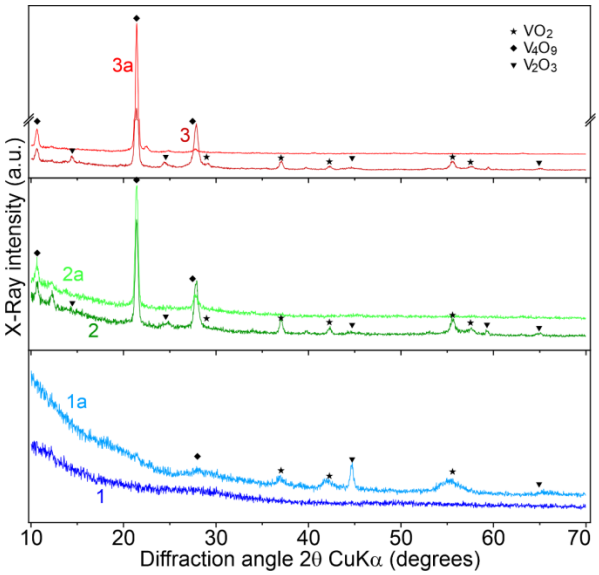

Fig. 1. X-ray diffraction patterns of sequentially deposited and annealed multiphase V_xO_y films, corresponding to samples 1, 1a, 2, 2a, 3, and 3a, illustrating the structural evolution through deposition and annealing cycles.

Subsequent annealing of this layer (sample 1a) induces partial crystallisation, as evidenced by the appearance of broad diffraction peaks corresponding to vanadium oxide phases, including VO_2, V_2O_3 and V_4O_9, as determined by phase analysis software and confirmed by Refs [5, 8, 13, 28]. This transformation suggests that annealing overcomes the energy barriers for crystal nucleation and growth in the initially amorphous structure.

The XRD pattern of the second V_xO_y layer (sample 2) reflects contributions from both the annealed bottom layer and the newly deposited top layer. Unlike the first deposition, the second layer benefits from more favourable growth conditions, likely due to homoepitaxial growth on the partially crystallized bottom layer. These conditions result in a pronounced crystalline structure with well-defined diffraction peaks. The annealing step further promotes recrystallization, resulting in the dominance of the V_4O_9 phase. This phase exhibits a strong texture along the <001> crystallographic direction, as evidenced by the presence of (001) and (002) reflections only in the XRD pattern.

A similar trend is observed during the third deposition and annealing cycle. The XRD pattern reveals a more pronounced crystalline structure in the newly deposited film (curve 3) and a well-defined texture in the annealed layer (curve 3a).

Figure 2 presents the atomic force microscopy height maps of the deposited and annealed V_xO_y films, highlighting the evolution of surface morphology. The XRD-observed sequential transformation of the crystalline structure correlates closely with the surface nanomorphology changes revealed by AFM, providing complementary insights into the film's structural development at different stages of deposition and annealing.

The first layer (sample 1) exhibits a non-uniform, wavy surface characterized by nearly flat hillocks, with identifiable grains up to 10 nm in size, and dendrite-like structures ranging from 150 to 300 nm located in the valleys. Upon annealing (sample 1a), the surface transforms, displaying nanograins with sizes between 30 and 80 nm, which cluster into aggregates approximately 300–350 nm in lateral dimensions.

Sequential deposition of the second layer (sample 2) produces a relatively flat surface, where nanoscale grains of 15–20 nm are barely discernible. Additionally, large-scale defects, as deep as the film's thickness, are observed, potentially corresponding to regions not fully covered by the newly deposited material. Subsequent annealing (sample 2a) significantly alters the morphology, resulting in the formation of well-defined grains with sizes in the range of 100–130 nm.

During the third cycle of deposition and annealing

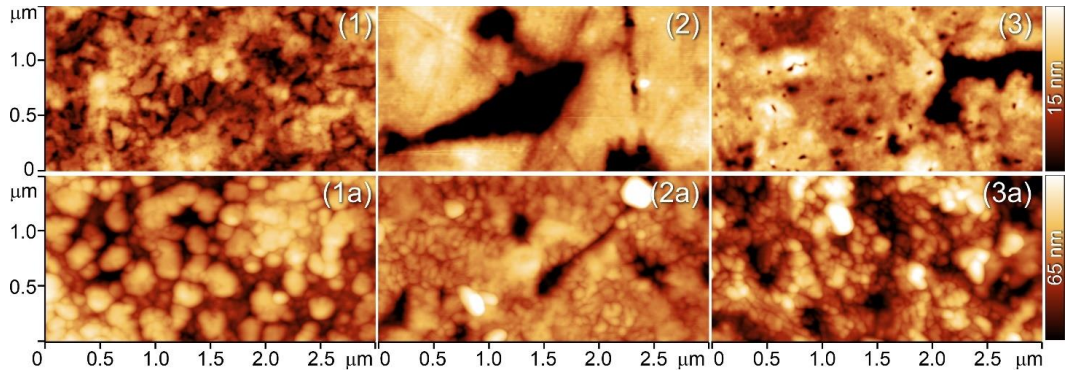

Fig. 2. The AFM height maps of the sequentially deposited and annealed multiphase V_xO_y films in samples 1, 1a, 2, 2a, 3 and 3a.

(samples 3 and 3a), a similar behaviour is observed. The deposition leads to surface flattening, while annealing promotes the development of grains, following a trend consistent with the transformations in stage 2.

The nanomechanical properties of samples 1, 1a, 2, 2a, 3, and 3a were investigated using the AFM nanoindentation option. Force-displacement curves obtained from AFM measurements were transformed into load-penetration curves through appropriate calibration procedures (Fig 3a) [29-31]. Since the surfaces are not uniform, a statistically significant number of nanomechanical measurements were collected across the surface. The most probable values, representing the peak of the data distribution, were selected for analysis to ensure reliability and reproducibility of the results. Hardness values were calculated as a function of maximum applied loading force and penetration depth, considering the projected area of the indent. Alternatively, the hardness values were checked by direct observation of nanindents in the tested surfaces, as shown in Figure 3b. Elastic moduli were determined by fitting the initial portion of the loading curve, where surface deformation is primarily elastic, using the Hertzian contact mechanics model. The results are summarized in Table 1.

The hardness and elastic modulus values show a clear correlation with the structural evolution of the V_xO_y films as observed through XRD and AFM surface morphology. Sample 1, with a predominantly amorphous structure and non-uniform surface morphology, exhibits the lowest hardness (0.9 GPa) and elastic modulus (9 GPa). These values reflect the weak interatomic bonding and structural disorder typical of amorphous films.

Annealing of sample 1 (sample 1a) results in partial crystallization, as evidenced by the formation of nanograins. This structural transition increases hardness (1.5 GPa) and elastic modulus (13 GPa), consistent with enhanced atomic ordering and reduced structural compliance.

Sample 2, representing a sequentially deposited layer, shows a significant improvement in mechanical properties (hardness: 3.3 GPa, elastic modulus: 17 GPa), accompanied by a more uniform grain size distribution. The observed enhancement likely arises from improved deposition conditions facilitated by the crystallized substrate. Subsequent annealing (sample 2a) yields well-defined grains and dramatic increases in hardness (18.0 GPa) and elastic modulus (270 GPa). These values align with the dominance of the crystalline V_4O_9 phase, as observed in XRD data. The role of crystalline texture in this improvement is significant; the well-ordered atomic arrangement along specific crystallographic directions, such as the observed <001> texture, enhances mechanical stability. This texture minimizes dislocation motion and improves load distribution under applied stress, resulting in higher hardness and elastic modulus values.

Samples 3 and 3a, representing the third deposition and annealing cycle, exhibit trends similar to stage 2. The as-deposited sample (sample 3) shows hardness and elastic modulus values (10.3 GPa and 165 GPa, respectively) slightly lower than the annealed state (sample 3a: 11.2 GPa and 263 GPa). The observed crystalline texture of previous layer further contributes to mechanical enhancement by providing well-aligned grains that resist deformation and optimize load transfer across

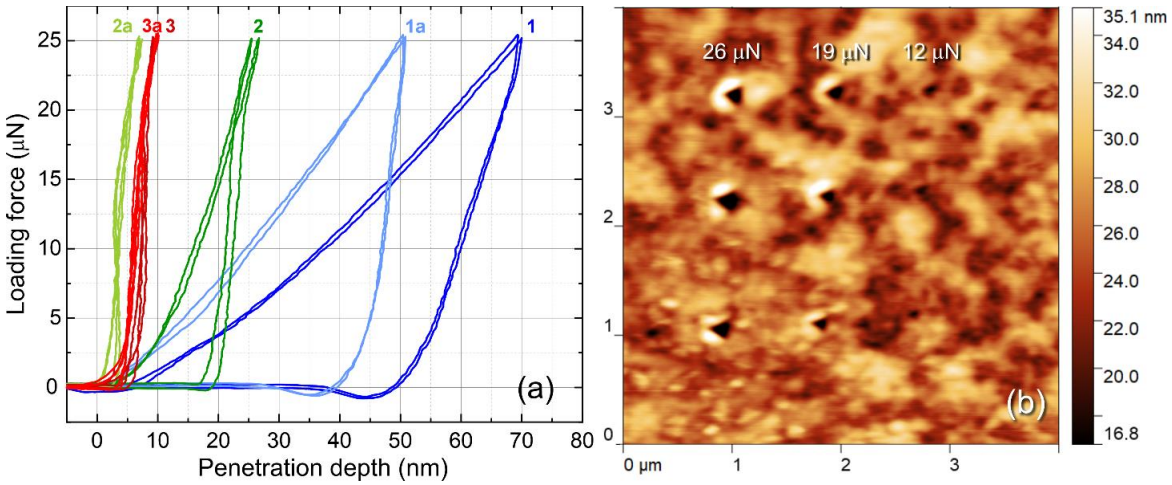

Fig. 3. Representative AFM nanoindentation curve pairs of samples with different V_xO_y layer numbers and annealing stages (a). Nano-indents in the first layer of V_xO_y (sample 1), produced by different maximum loading forces (b).

Table 1.

Parameters of the samples derived from the scanning probe study

Sample		Total thickness, nm	Grain size, nm	Hardness, GPa	Elastic modulus, GPa
1	as deposited	135	5-10 /150-300	0.9	9
1a	annealed		30-80 /300-350	1.5	13
2	as deposited	365	15-20	3.3	17
2a	annealed		100-130	18.0	270
3	as deposited	573	15-20	10.3	165
3a	annealed		30-60 /90-130	11.2	263

the material.

II. Raman spectroscopy

The Raman scattering spectra of the samples were studied at different excitation wavelength, λ_{exc} (457, 532, and 671 nm), because it may allow selectively probe (resonantly enhance) different phases, as have been demonstrated for various semiconductor and oxide composite (nano)structures [14, 32-35]. Moreover, in the case of thin films, longer wavelength usually can penetrate deeper into material, allowing certain degree of depth resolution [36]. The Raman spectra are summarized in Fig. 4. Sample 1 exhibited no features of any crystalline phase of VO_2, in agreement with the XRD data that detected purely amorphous material. The tiny Raman peaks in the range of other V_xO_y oxides may an indication of their formation in the process of Raman measurement, as a result of a slight local photoinduced crystallization of the film. Alternatively, these peaks may result from very small amounts of (nano- or micro) crystalline phase, not detectable by XRD, but resonantly enhanced in the Raman experiment [32, 33, 35]. Much more surprizing was observing no strong Raman peak for sample 1a (i.e. annealed first layer), because in the XRD this sample showed weak peaks of V_2O_3 (Fig.1). Therefore, one can assume that Raman spectroscopy is relatively not sensitive to this compound, at any of the excitation wavelengths used.

Upon deposition of the second amorphous oxide layer (sample 2), no significant changes occur in the XRD and Raman spectra. The significant weakening of the Raman peak of the Si substrate (at 520 cm^{-1}) at all three λ_{exc}'s indicates that the amorphous vanadium oxide rather strongly absorbs light in the whole visible range. Annealing of the two-layer structure (sample 2a) results in appearance of strong Raman peaks of VO_2 and weaker features in the range of other V_xO_y compounds (Fig. 4, a-c, curves 2a). This is in agreement with XRD that showed increase of the VO_2. From Fig.4, a-d we see that the shorter λ_{exc} produce stronger Raman signal of both VO_2 and other V_xO_y compounds. At λ_{exc} = 671 nm, only the feature at about 760 and 907 cm^{-1} are detected, which can be attributed to V_4O_9 [28]. The absence of these peaks in the Raman spectra at other λ_{exc} indicates that λ_{exc} = 671 nm (1.85 eV) is resonant for V_4O_9, but the Raman cross-section of this phase is obviously than that of VO_2 and V_3O_7 phases.

Upon deposition of the third amorphous layer (sample 3), again no Raman features of vanadium oxide are observed and the peak of Si substrate disappears completely. These observations can be explained by the strong optical absorption of the amorphous vanadious oxide, noticed above for the second layer.

Annealing of the three-layer structure (sample 3a) produces weaker and broader Raman peaks of the VO_2 phase (Fig.4 and Fig 5a), as compared to sample 2a, which may have negative effect on the parameter of MIT transitions of this multilayer film. On the other hand, the peaks of other V_xO_y phases are absent in this sample, which is presumably advantageous for MIT. In order to find out which of the two major differences detected for the samples 2a and 3a results in better parameters of the MIT transition, we have investigated MIT transition by two independent temperature-dependent methods –Raman spectroscopy and electrical resistivity measurements.

The possibility to observe MIT in VO_2 by means of vibrational (phonon) Raman spectroscopy is based on the fact that the Raman-active phonon modes of the isolator (semiconductor) type of the VO_2 structure gradually vanishes with increase of the sample temperature and transformation of the structure into the metallic anatase structure which does not exhibit measurable phonon Raman peaks [20]. Such dependence was also studied for the present samples and is illustrated in Fig. 5b by the set of spectra of sample 2a as a representative example. By plotting the integral intensity of one of the Raman peaks of the VO_2 phase, e.g. the one at 615 cm^{-1}, as a function of temperature in the range of MIT, one obtains a lineshape (hysteresis curves) qualitatively similar to the one more commonly derived from the temperature dependence of electrical resistivity [1, 5, 27]. In Fig. 6a the MIT curves derived from Raman and resistance are compared for samples 2a and 3a.

One fact that can be concluded from the Fig.6a is that

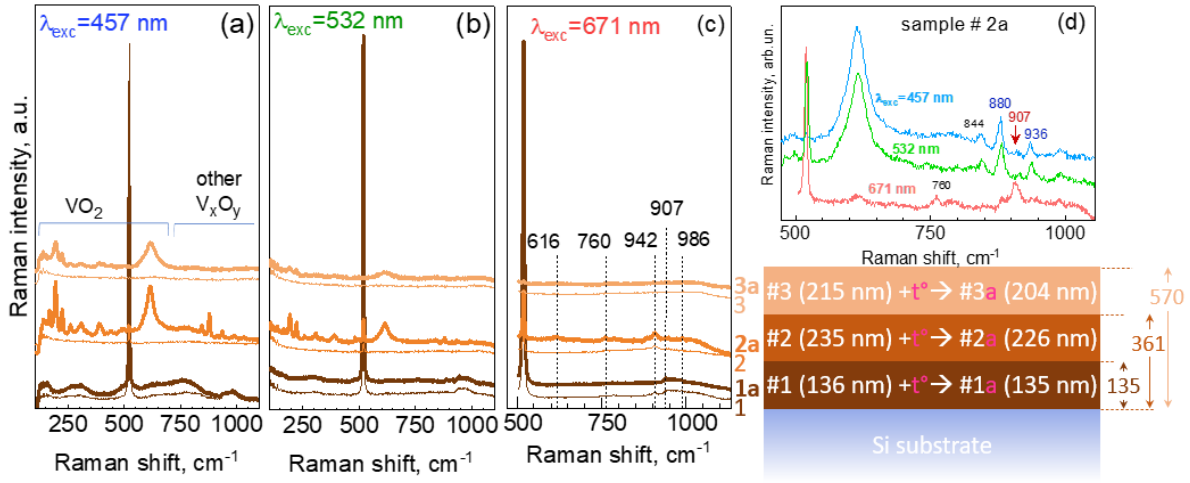

Fig. 4. Raman spectra of the samples 1-3a at different λ_{exc}, 457 (a), 532 (b), 671 nm (c), A and a comparative plot of the spectra obtained with different λ_{exc} for the same sample 2a (d). presented along with the schematic of the sample series.

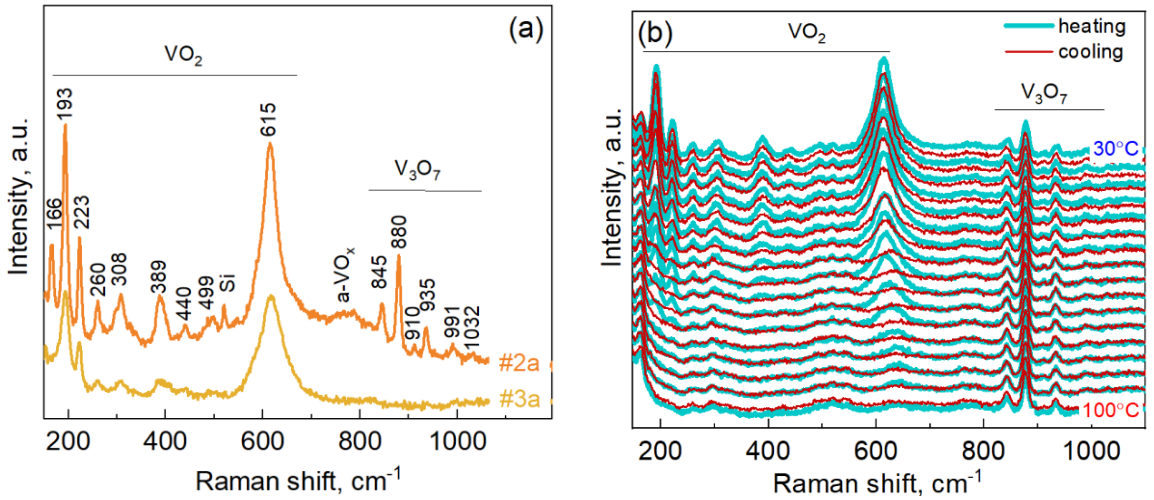

Fig. 5. (a) Raman spectrum of the samples 2a and 3a (λ_{exc}=457 nm) with indication of the peaks observed. (b) Temperature dependence of the Raman spectrum of sample 2a.

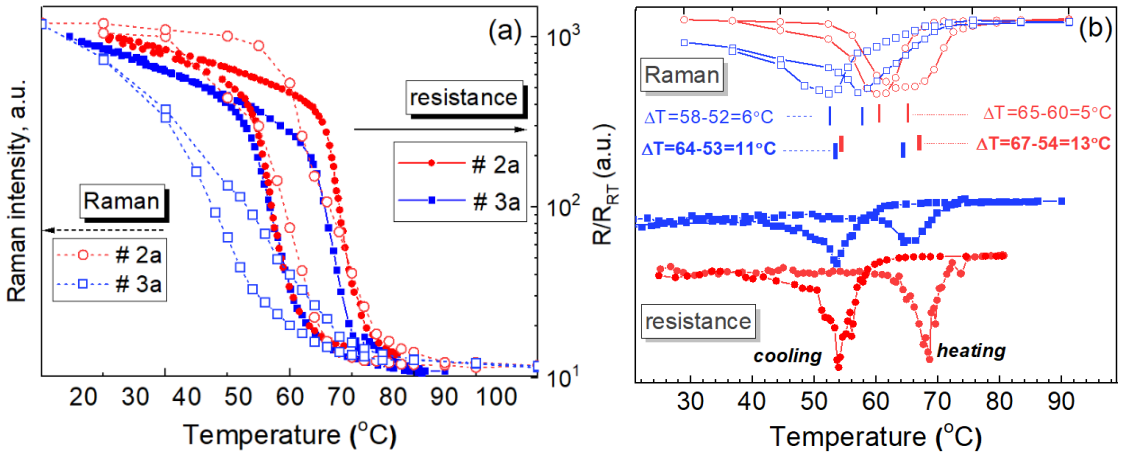

Fig. 6. (a) Comparison of the hysteresis curves obtained from Raman and electrical resistance measurements for samples 2a and 3a. (b) Derivatives of the hysteresis curves shown in (a), which present more obviously the T_{SMT} and ΔT values (the legend is the same as in (a)).

the sample 2a exhibit much better TCR value than sample 3a. This fact allows us to conclude that the superior quality of the VO_2 phase (recoded by Raman for the sample 2a) is more important for higher quality of the MIT transition than the absence of the "impurity phases", i.e. other V_xO_y oxides (recoded by Raman for the sample 3a).

The second important observation in the Fig.6a is that for the sample 2a that exhibit superior TCR of MIT, the hysteresis curves derived from Raman a well matching the curves derived from the electrical measurements. For the sample with worse TCR (3a), the Raman and resistance curves are pretty apart from each other – the structural transformation seem to occur faster than the drop of the resistance. Noteworthy is that the presence of the significant content of "impurity phases" of other V_xO_y oxides in the sample 2a does not hinder the MIT of the VO_2 phase to occur and the magnitude of the TCR and lineshape of the MIT hysteresis are comparable to numerous works on monophase VO_2 films [5-10].

Conclusions

Vanadium oxide films obtained by multiple deposition steps consisting of magnetron sputtering and annealing have been investigated. The highest TCR value was obtained after the annealing of second deposited layer. Inspection of the phonon Raman spectra indicate that the superior quality of the VO_2 phase is more important for higher quality of the MIT transition than the absence of the "impurity phases", i.e. other V_xO_y oxides. For the sample that exhibit superior TCR, the hysteresis curves derived from Raman are matching the curves derived from the electrical measurements. For the sample with worse TCR, the structural transformation reflected in Raman spectra occur faster than the drop in resistance.

The mechanical hardness of the first layer increases from 0.9 to 3.3 GPa, and with subsequent sputtering and annealing of the layers, it stabilizes at the level of 11-19 GPa. Based on XRD and Raman data on the content of various oxide phases in the samples, it was established that mechanical properties are the consequence of the structural transformation of the first layers from the quasi-amorphous to the nanocrystalline phase and the corresponding changes in the stoichiometry of vanadium oxide from the predominant phase V_4O_9 to VO_2, because VO_2 has a higher density and a more ordered structure than V_4O_9. The λ_{exc}=671 nm is found to be resonant and

selective for V_4O_9 detection, but its the cross-section of this phase is smaller than that of VO_2 and V_3O_7 phases at blue-green excitation.

The results obtained underscore the critical role of crystalline texture in governing the nanomechanical properties of V_xO_y films. Crystallization through annealing significantly improves hardness and elastic modulus due to the formation of well-defined grains with preferential orientation, which strengthen interatomic bonding and resist deformation mechanisms. Furthermore, the progressive enhancement in mechanical properties with sequential deposition cycles highlights the influence of substrate crystallinity and layer stacking in facilitating the development of optimal crystalline textures.

Acknowledgment

The work was financially supported by National Research foundation (grant # 2023.05/0022) for A.A.K, V.M.D, K.S., M.S.B., V.V.S., O.K and Priority Programme of NAS of Ukraine (1230) for other authors.

Korchoviy A.A. – PhD, senior researcher;
Lytvyn P.M. – PhD, head of department;
Dzhagan V.M. – Doctor of Science, Prof., Deputy Scientific Director of the Institute;
Gudymenko O.Y. – PhD, senior researcher;
Svezhentsova K.V. – PhD, senior researcher;
Boltovets M.S. – PhD, senior researcher;
Strelchuk V.V. – Doctor of Science, Prof., leading researcher;
Kolesnikov O.M. – researcher;
Isaieva O.F. – PhD, researcher;
Yefanov V.S. – PhD, senior researcher;
Melnik V.P. – Doctor of Science, Prof., Director of the Institute;
Romanyuk B.M. – Doctor of Science, Prof., head of department.

[1] P. Hu, P. Hu, T.D. Vu, M. Li, S. Wang, Y. Ke, X. Zeng, L. Mai, Y. Long, *Vanadium Oxide: Phase Diagrams, Structures, Synthesis, and Applications,* Chem Rev., 123, 4353 (2023); https://doi.org/10.1021/acs.chemrev.2c00546.

[2] M.Ya. Valakh, V.O. Yukhymchuk, V.M. Dzhagan, O.F. Isaieva, V.S. Yefanov, B.M. Romanyuk, *Variation of the Metal-Insulator Phase Transition Temperature in VO_2: An Overview of Some Possible Implementation Methods,* Semicond. Physics, Quantum Electronics & Optoelectronics, 27 (2), 136 (2024); https://doi.org/10.15407/spqeo27.02.136.

[3] Y. Skorenkyy, O. Kramar, Y. Dovhopyaty, *Strong Correlation Effects in Vanadium Oxide Films,* Physics and Chemistry of Solid State, 23(1), 62 (2022); https://doi.org/10.15330/pcss.23.1.62-66.

[4] F. Urena-Begara, A. Crunteanu, J. Raskin, *Raman and XPS Characterization of Vanadium Oxide Thin Films with Temperature,* Appl. Surf. Sci., 403, 717 (2017); https://doi.org/10.1016/j.apsusc.2017.01.160.

[5] S. Chouteau, S. Mansouri, M. Lemine, O. Ne, A.O. Suleiman, B. Le Drogoff, M. Chaker, *Investigation of the Metal-to-Insulator Transition of N-doped VO_2 (M1) Thin Films,* Appl. Surf. Sci., 554, 149661 (2021); https://doi.org/10.1016/j.apsusc.2021.149661.

[6] A. Romanyuk, R. Steiner, L. Marot, P. Oelhafen, *Temperature-Induced Metal – Semiconductor Transition in W-doped VO_2 Films Studied by Photoelectron Spectroscopy,* Solar Energy Materials & Solar Cells, 91, 1831 (2007); https://doi.org/10.1016/j.solmat.2007.06.013.

[7] S. Lysenko, V. Vikhnin, A. Rúa, F. Fernández, H. Liu, *Critical Behaviour and Size Effects in Light-Induced Transition of Nanostructured VO_2 Films,* Phys Rev B, 82, 205425 (2010); https://doi.org/10.1103/PhysRevB.82.205425.

[8] K.L. Gurunatha, S. Sathasivam, J. Li, M. Portnoi, I.P. Parkin, I. Papakonstantinou, *Combined Effect of Temperature Induced Strain and Oxygen Vacancy on Metal-Insulator Transition of VO_2 Colloidal Particles,* Adv Funct Mater., 30 (49), 2005311 (2020); https://doi.org/10.1002/adfm.202005311.

[9] E. Radue, E. Crisman, L. Wang, S. Kittiwatanakul, J. Lu, S.A. Wolf, R. Wincheski, R.A. Lukaszew, I. Novikova, Effect of a Substrate-Induced Microstructure on the Optical Properties of the Insulator- Metal Transition Temperature in VO_2 Thin Films, J. Appl. Phys., 113, 233104 (2013); https://doi.org/10.1063/1.4811689.

[10] M. Becker, J. Kessler, F. Kuhl, S.L. Benz, L. Chen, A. Polity, P.J. Klar, S. Chatterjee, *Phase Control of Multivalent Vanadium Oxides VO_x by Ion-Beam Sputter-Deposition,* Phys. Stat. Sol (a), 219, 2100828 (2022); https://doi.org/10.1002/pssa.202100828.

[11] A. Rana, A. Yadav, G. Gupta, A. Rana, *Infrared Sensitive Mixed Phase of V_7O_{16} and V_2O_5 Thin-Films,* RSC Adv. 13, 15334 (2023); https://doi.org/10.1039/d3ra00752a.

[12] N. Kumar, A. Rúa, J. Lu, F. Fernández, S. Lysenko, *Ultrafast Excited-State Dynamics of V_3O_5 as a Signature of a Photoinduced Insulator-Metal Phase Transition,* Phys Rev Lett., 119, 057602 (2017); https://doi.org/10.1103/PhysRevLett.119.057602.

[13] S. Yamazaki, C. Li, K. Ohoyama, M. Nishi, M. Ichihara, H. Ueda, Y. Ueda. *Synthesis, Structure and Magnetic Properties of V_4O_9 – A Missing Link in Binary Vanadium Oxides,* J. Solid State Chem., 183, 1496 (2010); https://doi.org/10.1016/j.jssc.2010.04.007.

[14] C. Zhang, Q. Yang, C. Koughia, F. Ye, M. Sanayei, S. Wen, S. Kasap, *Characterization of Vanadium Oxide Thin Films with Different Stoichiometry Using Raman Spectroscopy,* Thin Solid Films, 620, 64 (2016); https://doi.org/10.1016/j.tsf.2016.07.082 .

[15] A Subrahmanyam, Y B. K. Reddy, and C L Nagendra. *Nano-Vanadium Oxide Thin Films in Mixed Phase for Microbolometer Applications,* J. Phys. D: Appl. Phys., 41, 195108 (2008); https://doi.org/10.1088/0022-3727/41/19/195108.

[16] M. Abdel-Rahman, M. Zia and M. Alduraibi, Temperature-Dependent Resistive Properties of Vanadium Pentoxide/Vanadium Multi-Layer Thin Films for Microbolometer & Antenna-Coupled Microbolometer Applications, Sensors, 19, 1320 (2019); https://doi.org/10.3390/s19061320.

[17] P.M. Lytvyn, V.M. Dzhagan, M.Ya. Valakh, A.A. Korchovyi, O.F. Isaieva, O.A. Stadnik, O.A. Kulbachynskyi, O.Yo. Gudymenko, B.M. Romanyuk, V.P. Melnik, *Nanomechanical Properties of Polycrystalline Vanadium Oxide Thin Films of Different Phase Composition,* Semiconductor Physics, Quantum Electronics & Optoelectronics, 26, 388 (2023); https://doi.org/10.15407/spqeo26.04.388.

[18] V.M. Dzhagan, M. Ya Valakh, O.F. Isaieva, V.O. Yukhymchuk, O.A. Stadnik, O. Yo Gudymenko, P.M. Lytvyn, O.A. Kulbachynskyi, V.S. Yefanov, B.M. Romanyuk, V.P. Melnik, *Raman Fingerprints of Different Vanadium Oxides as Impurity Phases in VO_2 Films,* Optical Materials, 148, 114894 (2024); https://doi.org/10.1016/j.optmat.2024.114894.

[19] A.A. Efremov, B.M. Romaniuk, V.P. Melnyk, O.A. Stadnik, T.M. Sabov, O.A. Kulbachinskiy, O.V. Dubikovskiy. *Study of Fractality Nature in VO_2 Films and its Influence on Metal-Insulator Phase Transition,* Semiconductor Physics, Quantum Electronics & Optoelectronics, 27 (1), 028 (2024); https://doi.org/10.15407/spqeo27.01.028.

[20] V.V. Strelchuk, O.F. Kolomys, D.M. Maziar, V.P. Melnik, B.M. Romanyuk, O.Y. Gudymenko, O.V. Dubikovskyi, O.I. Liubchenko, Effect of Structural Disorder on the Modification of V–V and V–O Bond Lengths at the Metal-Dielectric Phase Transition in VO_2 Thin Films, Materials Science in Semiconductor Processing, 174, 108224 (2024); https://doi.org/10.1016/j.mssp.2024.108224.

[21] V. Melnik, I. Khatsevych, V. Kladko, A. Kuchuk, V. Nikirin, B. Romanyuk, *Low-Temperature Method for Thermochromic High Ordered VO_2 Phase Formation,* Mater Lett. 68, 215 (2012); https://doi.org/10.1016/j.matlet.2011.10.075 .

[22] Y. Goltvyanskyi, I. Khatsevych, A. Kuchuk, V. Kladko, V. Melnik, P. Lytvyn, V. Nikirin, B. Romanyuk, *Structural Transformation and Functional Properties of Vanadium Oxide Films after Low-Temperature Annealing,* Thin Solid Films, 564, 179 (2014); https://doi.org/10.1016/j.tsf.2014.05.067.

[23] D. Singh, B. Viswanath, *In Situ Nanomechanical Behaviour of Coexisting Insulating and Metallic Domains in VO_2 Microbeams,* J. Mater. Sci., 52 (10), 5589 (2017); https://doi.org/10.1007/s10853-017-0792-4.

[24] H. Guo, K. Wang, Y. Deng, Y.Oh, S.A. Syed Asif, O.L. Warren, Z.W. Shan, J. Wu, A.M. Minor, *Nanomechanical Actuation from Phase Transitions in Individual VO_2 Micro-Beams,* Appl. Phys. Lett., 102, 231909 (2013); https://doi.org/10.1063/1.4810872.

[25] Y.A. Birkhölzer, K. Sotthewes, N. Gauquelin, L. Riekehr, D. Jannis, E. Van Der Minne, Y. Bu, J. Verbeeck, H.J.W. Zandvliet, G. Koster, G. Rijnders, *High-Strain-Induced Local Modification of the Electronic Properties of VO_2 Thin Films,* ACS Appl. Electron. Mater., 4 (12), 6020 (2022); https://doi.org/10.1021/acsaelm.2c01176.

[26] M. Mazur, A. Lubańska, J. Domaradzki, D. Wojcieszak, *Complex Research on Amorphous Vanadium Oxide Thin Films Deposited by Gas Impulse Magnetron Sputtering,* Appl. Sci., 12 (18), 8966 (2022); https://doi.org/10.3390/app12188966.

[27] V.P. Kladko, V.P. Melnik, O.I. Liubchenko, B.M. Romanyuk, O.Y. Gudymenko, T.M. Sabov, O. V. Dubikovskyi, Z. V Maksimenko, O. V Kosulya, O.A. Kulbachynskyi, P.M. Lytvyn, O.O. Efremov, *Semiconductor Physics Phase Transition in Vanadium Oxide Films Formed by Multistep Deposition,* Semiconductor Physics, Quantum Electronics & Optoelectronics, 24, 362 (2021); https://doi.org/10.15407/spqeo24.04.362.

[28] R. Nilsson, T. Lindblad, A. Andersson, *Ammoxidation of Propane Over Antimony Vanadium-Oxide Catalysts,* Journal of Catalysis, 148, 501 (1994); https://doi.org/10.1006/jcat.1994.1236.

[29] C.A. Clifford, M.P. Seah, Quantification Issues in the Identification of Nanoscale Regions of Homopoly-mers Using Modulus Measurement Via AFM Nanoindentation. Appl. Surf. Sci., 252,1915 (2005); https://doi.org/10.1016/j.apsusc.2005.08.090.

[30] T. Chudoba, M. Griepentrog, A. Dück et al., *Young's Modulus Measurements on Ultra-Thin Coatings,* J. Mater. Res., 19, 301 (2004); https://doi.org/10.1557/jmr.2004.19.1.301.

[31] Y. Liu, I. Sokolov, M.E. Dokukin, Y. Xiong, P. Peng, *Can AFM be Used to Measure Absolute Values of Young's Modulus of Nanocomposite Materials Down to the Nanoscale?,* Nanoscale, 12 (23), 12432 (2020); https://doi.org/10.1039/D0NR02314K.

[32] V. Dzhagan, B. Kempken, M. Valakh, J. Parisi, J. Kolny-Olesiak, *DRT Zahn Probing the Structure of $CuInS_2$-ZnS Core-Shell and Similar Nanocrystals by Raman Spectroscopy,* Applied Surface Science, 395, 24 (2017); https://doi.org/10.1016/j.apsusc.2016.08.063.

[33] O. Selyshchev, Y. Havryliuk, M.Ya. Valakh, V.O. Yukhymchuk, O. Raievska, O.L. Stroyuk, V. Dzhagan, and D.R.T. Zahn, Raman and X-ray Photoemission Identification of Colloidal Metal Sulfides as Potential Secondary Phases in Nanocrystalline Cu_2ZnSnS_4 Photovoltaic Absorbers, ACS Appl. Nano Mater., 3 (6), 5706 (2020); https://doi.org/10.1021/acsanm.0c00910.

[34] A.O. Suleiman, S. Mansouri, N. Émond, B. Le Drogoff, T. Bégin, J. Margot, M. Chaker, *Probing the Role of Thermal Vibrational Disorder in the SPT of VO_2 by Raman Spectroscopy,* Sci Rep., 11, 1620 (2021); https://doi.org/10.1038/s41598-020-79758-1.

[35] V. Dzhagan, A.P. Litvinchuk, M.Y. Valakh, D.R.T. Zahn, *Phonon Raman Spectroscopy of Nanocrystalline Multinary Chalcogenides as a Probe of Complex Lattice Structures*, J. Phys.: Condensed Matter, 35, 103001 (2022); https://doi.org/10.1088/1361-648X/acaa18.

[36] C.W. Chang, M.H. Hong, W.F. Lee et al., Micro-Raman Characterization of Ge Diffusion and Si Stress Change in Thin Epitaxial $Si_{1-x}Ge_x$ Layers on Si (100) After Rapid Thermal Annealing, J. Mater. Research., 27(9), 1314 (2012); https://doi.org/10.1557/jmr.2012.88.

А.А. Корчовий, П.М. Литвин, В.М. Джаган, О.Й. Гудименко, К.В. Свеженцова, М.С. Болтовець, В.В. Стрельчук, О.М Колесніков, О.Ф. Ісаєва, В.С. Єфанов, В.П. Мельник, Б.М. Романюк

Наномеханічні та коливні властивості тонких плівок оксиду ванадію, отриманих методом багатоступінчастого осадження

Інститут фізики напівпровідників імені В.Є. Лашкарьова НАН України, Київ, Україна, svezhentsova@ukr.net

Тонкі плівки оксиду ванадію були виготовлені за допомогою багатоетапного процесу осадження, що включає магнетронне розпилення та послідовний відпал. Досліджено структурні, коливні та наномеханічні властивості плівок, для з'ясування впливу фазового складу на якість фазового переходу метал-ізолятор (MIT). Рентгенівська дифракція (XRD) і спектроскопія комбінаційного розсіювання виявили структурну еволюцію від квазіаморфних до нанокристалічних фаз після відпалу, з домінуванням переходу від VO_2 до текстурованого V_4O_9. Спостережувані фазові переходи супроводжуються зростанням твердості з 0,9 ГПа в аморфному першому шарі до 11–18 ГПа у всіх багатошарових (кристалічних) структурах. Підвищення механічної міцності пояснюється розвитком добре впорядкованої кристалічної текстури, що покращує міжатомні зв'язки і опір деформації. Раманівські коливні спектри, отримані на різних довжинах хвиль збудження, виявили резонансну чутливість до різних оксидних фаз, включаючи мінорну фазу V_3O_7, яка не виявляється за допомогою XRD, і селективний резонансний прояв фази V_4O_9 лише зі збудженням 671 нм. Температурна залежність Раманівських спектрів та питомого електричного опору показали кращі характеристики MIT для зразків із вищим вмістом VO_2, незважаючи на присутність в цих зразках інших фаз V_xO_y. Це вказує на визначальну роль структурного впорядкування для механічних і функціональних властивостей плівок оксиду ванадію, пропонуючи цінну інформацію для оптимізації методів обробки для передових електронних і оптичних застосувань.

Ключові слова: Оксид ванадію, VO_2, V_4O_9, V_3O_7, Раманівська спектроскопія, рентгенівська дифракція, наноіндентування, перехід метал-ізолятор, фазовий перехід.